Reconstruction of annual accumulation rate on firn synchronizing H_2O_2 concentration data with an estimated temperature record

Jandyr M. Travassos[1], Saulo S. Martins[2], Mariusz Potocki[4,5], and Jefferson C. Simões[3,4]

[1]Graduate Program in Geophysics, Universidade Federal do Pará (UFPA), Rua Augusto Corrêa n. 01, Belém, Pará, Brazil
[2]Graduate Program in Geology, Universidade Federal Rural do Rio de Janeiro (UFRRJ). BR-465 Km 7, Seropédica, Brazil
[3]Centro Polar e Climatico, Universidade Federal do Rio Grande do Sul (UFRGS), Porto Alegre, Brazil
[4]Climate Change Institute, University of Maine, Orono, USA
[5]School of Earth and Climate Sciences, University of Maine, Orono, ME 04469, USA

Correspondence: Saulo S. Martins (ssmsaulo@gmail.com)

Abstract. This work deals with ~~two distinct datasets, a well preserved hydrogen peroxide, H$_2$O$_2$, concentration data from firn cores at a high deposition location and a temperature time series, estimated from the daily records from four Antarctic stations around the Antarctic Peninsula. With them we have produced~~ the reconstruction of firn layer thicknesses at the deposition time from its observed thickness in ice cores, thus reconstructing the annual accumulation, yielding a time scale, an ice-core chronology~~, for the 133m deep borehole DP-07-1 from Plateau Detroit, Antarctic Peninsula. We constructed the chronology through a non-linear pairing transformation of the two series, based entirely on mathematical optimization, compensating the peroxide frequency scaling, reflecting the gradual thinning of the annual firn layers with depth. We resorted to~~. We employed a dynamic time warping algorithm to find an optimal ~~alignment between the two data series~~, ~~allowing for the thinning of the annual firn layers with depth and the estimation of their original thicknesses at time of deposition. The core chronology spanning from Jan-1980 to Dec-2010 for the borehole reach,~~ non-linear, alignment between a ~~time frame of a mere 30 years period, revealing a fairly stable 11 year average for the accumulation rate of 2.5 m w.e./y~~ H_2O_2 concentration data series from 98m worth of ice cores of a borehole on the central ice divide of Detroit Plateau, and an estimated local temperature time series. The viability and the physical reliability of the procedure are rooted both in the robustness of the seasonal marker H_2O_2 on a high accumulation context, which brought the entire borehole to within the operational life span of four Antarctic stations around the Antarctic Peninsula. The process was heavily based on numerical optimization, producing a mathematically sound match between the two series, able to estimate efficiently the annual layering on the entire data section at once, being disposition-free. Results revealed a high annual accumulation rate of $a_N = 2.8\,\mathrm{mweq/y}$, of the same order and highly correlated with the corresponding reported elsewhere for Bruce Plateau, a possible indication that the Northern tip of the Antarctic Peninsula has been under a high snow accumulation regime, twice as large as Gomez's further South.

1 Introduction

Ice cores provide a continuous record of climatic and environmental data series based on some physical and chemical properties of ice, reflecting past atmospheric composition and climatic variability, (*e.g.* ~~Masson-Delmotte et al. (2006)~~ Masson-Delmotte et al., 2006

). Snow is deposited on the ice surface being gradually compressed into firn and ice, having the ability to preserve a very reliable climate record, with a low risk of missing years, provided that the accumulation rate is sufficiently high. A key issue in the

25 paleoclimatic reconstruction is dating the stratigraphic sequence through different techniques which include 1-D to 3-D flow models (Nye, 1952; Dansgaard and Johnsen, 1969; Gillet-Chaulet et al., 2012; Passalacqua et al., 2016), counting of cycles of seasonally varying quantities, reference horizons, most commonly layers of high concentrations of sulphuric acid related to volcanic events (Vinther et al., 2006), and layer identification through peaks of radiative isotopes (Vinther et al., 2006; Cuffey and Paterson, 2010). Often those techniques are combined, *e.g.*, incorporating stable water isotope $\delta^{18}O_{atm}$ to an ice flow

30 model (Capron et al., 2010).

The Hydrogen peroxide (H_2O_2) is produced by photochemical reactions in natural waters exposed to solar irradiation, surficial and atmospheric. It is the most stable of the reactive oxygen species created in the atmosphere through a chemical reaction requiring ultraviolet light. A kinetic model explained 76.7% of the variation in H_2O_2 concentrations is due to solar irradiance and temperature variation only (Sigg and Neftel, 1988). In particular that production in Antarctica has a conspicuous regular

35 seasonality resulting from cycles of complete darkness in midwinter to 24h daylight in midsummer. This gives a phenomenological basis for a quasi-sinusoidal variability in H_2O_2 atmospheric concentration with maxima occurring during the sunlit summer (Steig et al., 2005; Frey et al., 2006). The H_2O_2 ~~reportedly may reach a summer-to-winter ratio of 5 in high accumulation rate ice cores from atmospheric concentration ratios of ~ 50 (Sigg and Neftel, 1988; Hutterli et al., 2003; Frey et al., 2006). The H_2O_2~~ is a particularly robust marker for ice cores at high accumulation sites in Antarctica (Sigg and Neftel, 1988; Frey

40 et al., 2006) where post-depositional losses are minimized resulting in excellent preservation of the records, with summer-to-winter ratios in excess of 5 (Sigg and Neftel, 1988; Hutterli et al., 2003; Frey et al., 2006).

The H_2O_2 concentration data comes from ice cores extracted from borehole DP-07-1 drilled in December 2007 at the ice divide of ~~Plateau Detroit (PD~~Detroit Plateau (DP), at $64°05'07''S$, $59°38'42''W$, 1930m above sea level. DP-07-1 reveals well-resolved seasonal cycles of H_2O_2 concentration data on a context of a very high deposition rate (Potocki et al., 2016).

45 We take advantage of the observed strong seasonality in the H_2O_2 record to estimate a core time scale spanning the entire firn horizon. That is done through the synchronization of the concentration data to an estimated temperature time series at the borehole location.

The ~~reported strong seasonality on the production~~ maxima of H_2O_2 ~~in Antarctica, allow us to concentrate on the yearly cycles of the~~ production and of surficial atmospheric temperature ~~alone as a proxy for the solar irradiation~~occur during the

50 sunlit months of the austral summer, allowing us to seek a correlation between their respective maxima. Obviously they do not necessarily occur at the same time but they do during summertime, the time difference between them being a fraction of an year. A temperature record at the borehole location on ~~PD~~ DP may be estimated by interpolating the historical temperature recordings from six Antarctic stations, not too far from ~~PD~~DP: Bellingshausen, Esperanza, Faraday, Marambio, O'Higgins and Rothera, which have almost continuous meteorological observations from the late 1950's. We have discarded Belling-

55 shausen and O'Higgins, the first for being heavily biased by maritime conditions, the second due to a relatively short record with a sizable gap in it, leaving us with four stations forming the vertices of a polygon having ~~PD~~ DP within its perimeter. Only Marambio lies on the eastern side, which may imply some unknown bias towards the western temperature regime of
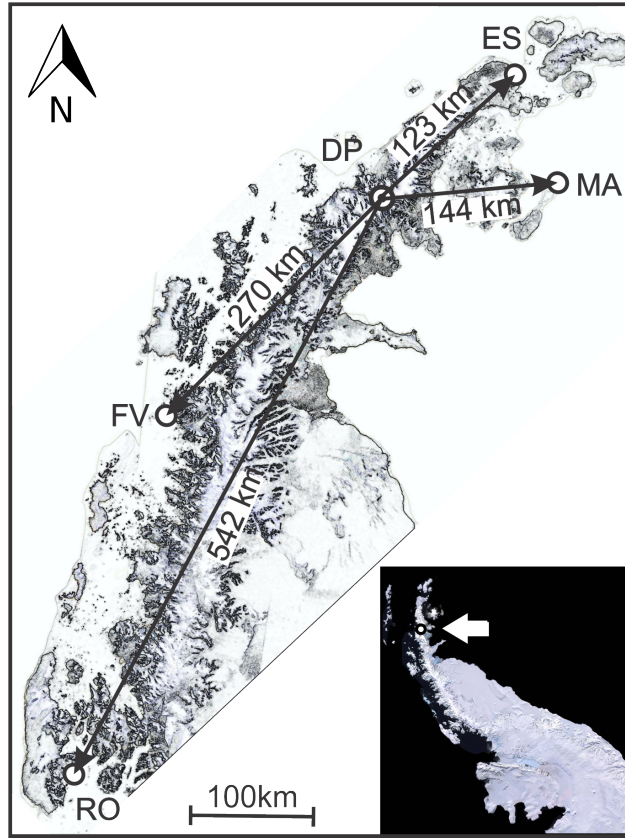
Figure 1. The four Antarctic Stations, Esperanza (ES), Marambio (MA), Faraday-Vernadsky (FV) and Rothera (RO), and ~~of~~ the borehole at ~~PD~~DP, on the Northern Antarctica Peninsula. The white arrow in the right lower corner inset shows the location of ~~PD~~ DP on the Peninsula. Both maps were modified from a pan-sharpened scene (RGBREF_x − 2550000y + 1350000) of the Landsat Image Mosaic of Antarctica (LIMA) by USGS https://lima.usgs.gov/

.

the Antarctic Peninsula. Figure ~~??~~1 shows the locations of the Antarctic stations on an outline of the Northern Antarctica Peninsula.

60   The synchronization of the concentration data to a temperature series is warranted here due to the local accumulation rate, high enough to bring the entire firn horizon deposition period to within the reach of the four stations operational span. Both data series independently follow the same seasonal variation, the passing of the years, nevertheless in their particular manners; the H_2O_2 concentration displays a frequency scaling with depth, a result from the accumulated vertical strain, whereas the temperature series has an uniform frequency behavior. The frequency scaling reflects the gradual thinning of the annual firn

65 layers, which manifests itself as a frequency chirp in the H_2O_2 concentration series.

    We have allowed for the frequency scaling of the peroxide concentration series in relation to the uniform frequency temperature content by resorting to dynamic time warping (DWT). The DWT is a fast and efficient algorithm for finding an optimal

alignment between two sequences through a non-linear warping of one onto the other along the time/depth axis (Rabiner et al., 1978; Sakoe and Chiba, 1978). We have worked with standardized versions of the peroxide and temperature series, using the

70 distance between them as a measure for their resemblance (Rabiner et al., 1978; Sakoe and Chiba, 1978). Once this is optimally found, the peroxide series becomes warped onto the temperature series thus allowing for the observed frequency scaling.

Notwithstanding DTW has begun associated with speech recognition (Rabiner et al., 1978; Sakoe and Chiba, 1978; Gilbert et al., 2010) it has proved to be useful in several other applications. They encompass handwriting recognition (Kolhe et al., 2009), image and shape matching (Wang et al., 1997; Latecki et al., 2007), analysis and classification the land cover of remotely

75 sensed images (Verbesselt et al., 2010; Xue et al., 2014), gene expression and protein structure (Criel and Tsiporkova, 2005; Legrand et al., 2008) and even brain activity (Chaovalitwongse and Pardalos, 2008). Speech recognition has been used to detect layers in Greenland deep ice cores, using a Hidden Markov Model (Winstrup and Svensson, 2010).

This work shows that DTW is also particularly fit for compensating the peroxide frequency scaling with depth, realigning it to a temperature data time series and, at the same time, quantifying their dissimilarities. We have used the constant spectral

80 content of the temperature data series as a reference in the pairing transformation through mathematical optimization, thus yielding an estimate of a relation of depth to time without human intervention. Moreover the procedure has also confirmed a very high deposition rate for the entire firn horizon at ~~PD~~DP.

2 The Data Sets

We deal with two independent data sets, a H_2O_2 concentration from the 133m deep borehole and a temperature time series

85 estimated at ~~PD~~DP. We have also collected a record of the stable water isotope deuterium, which was not used due to its poor seasonal variability (Potocki et al., 2016). The borehole yielded intact ice cores down to $z = 109.3 \pm 0.5$m, from where brittle ice begun. The borehole temperature was fairly stable at $-14.2 \pm 0.1\,°$C at a depth of 10m~~, conductivity measurements on ice cores down to 20m had a modal value of 40.4μS/cm~~. Depths in the borehole are measured with the origin at the surface and the vertical z-axis pointing downwards.

90 The temperature time series at borehole location was estimated through an interpolation procedure on a data set of continuous temperature readings since January 1st, 1970, at four Antarctic stations in Antarctic Peninsula. We are going to show below that the entire firn layer was accumulated in a shorter time span than the > 45y of estimated temperature time series.

2.1 The H_2O_2 Concentration Data

The H_2O_2 concentration data ~~has a high resolution sampling, averaging to~~ was retrieved from the first 98m of ice cores with

95 high-resolution sampling, with an average of 36 samples/year~~along the 98m of ice cores. It has~~. It is a robust seasonal signal, well preserved for the entire depth range of ice cores (Potocki et al., 2016). As for other ice cores at high accumulation sites across West Antarctica, it is possible to establish a time scale for the core through straightforward counting of the annual cycles (Sigg and Neftel, 1988; Frey et al., 2006).
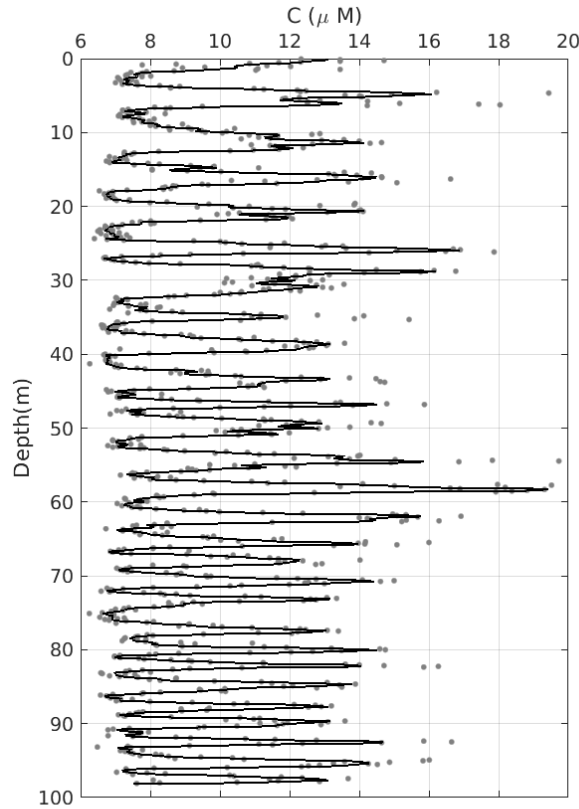
Figure 2. The grey dots are the raw data $C(z)$, the solid line is their smoothed version $\mathcal{C}(z)$, both expressed in μM. For the sake of ~~of~~ visualization, we have omitted just two data points with concentration $C(z) > 20\mu$M at depths ≈ 5m.

The H$_2$O$_2$ concentration record, $C(z)$ has a considerable noise content throughout, which has to be minimized making its seasonal signal conspicuous. We produce a smooth data series $\mathcal{C}(z)$ by robust fitting on $C(z)$ through a loess nonparametric method (Cleveland and Grosse, 1991). The Figure 2 shows both $C(z)$ and $\mathcal{C}(z)$ in micro molar (μM) concentration. It is easy to see the seasonal signal in $\mathcal{C}(z)$ as well as the effect of the accumulated vertical strain with depth on the annual firn layers. The latter manifests itself as a gradual thinning of the annual firn layers.

Notwithstanding some residual noise left on $\mathcal{C}(z)$ straightforward counting of its peaks and troughs suggests the first ~~100m~~ 98m were probably accumulated in its entirety from the beginning of the 80's. Straightforward division of the total depth span by the number of peaks indicates a very high deposition rate at ~~PD~~DP, a topic we are going to address below.

2.2 Estimating a Temperature Time Series at Detroit Plateau

The four stations shown in Figure 1 have distinct sampling on temperature, varying from 1 to 8 readings/day. We set the beginning of the estimated temperature record to January 1st, 1970, from this date onward all four stations have continuous temperature readings. The end of the record is set on December 29th, 2010, three years after the core was drilled at DP. These limits yield a time span wide enough to safely encompass the entire deposition period of the firn horizon.

We interpolated the daily temperature time series from the four stations shown in Figure 1 through Delaunay triangulation, having the DP borehole sea-level projection inside the convex hull formed by the station set. That is a linear interpolation weighted by the inverse of the horizontal distance between a given station to the borehole projection. It is noteworthy all stations but Marambio are located on the occidental part of the Peninsula, but is shares the largest weights with Esperanza. Some bias towards the western climate regime somewhat compensated by Marambio is thus expected, a fact we have to leave with anyway.

Only the maximum daily temperature reading at each station was used in the interpolation process. The sea-level interpolated time series at DP, $T(t)$, is further corrected to the height of DP at 1930 m asl, with a lapse rate in temperature with altitude of $-0.55°C/100$m (Rolland, 2003). Even taking care to obtain the best temperature estimates from the interpolation process at DP, the accuracy of a particular temperature estimate is not crucial to our results as we use only the location in time of a given summertime peak temperatures for synchronization.

We alleviated aliasing due to the temperature sampling by applying a two-day low-pass filter to $T(t)$, a series with 14973 data points, far more than the 985 data points of $C(z)$. We made the number of data points in $\mathcal{T}(t)$ similar to those in $C(z)$ by decimating the former by $15\times$. Again we avoided aliasing and conspicuously reduced noise in $\mathcal{T}(t)$ by low-pass filtering the decimated data series, using an eight order Chebyshev filter. We compensated the amplitude losses incurred throughout the conditioning process by a constant multiplicative gain, bringing the amplitudes of the filtered temperature time series somewhat back to the original levels of the unfiltered $T(t)$. The multiplicative factor is estimated in successive time windows as the quotient of the envelope of the original $T(t)$ by envelope of the not gained version of $\mathcal{T}(t)$. From now on $\mathcal{T}(t)$ will refer to the gained temperature time series.

Figure 3 shows the decimated $T(t)$ and $\mathcal{T}(t)$, spanning over 41 years. The time series $T(t)$ is quite noisy as one would have expected it to be but the $\mathcal{T}(t)$ proves to be a robust depiction of the annual summer-winter cycles. It has a smaller amplitude than that of $T(t)$, which is hardly an issue here as we are not looking for individual temperature figures but rather a reliable counter on the passing of the years.
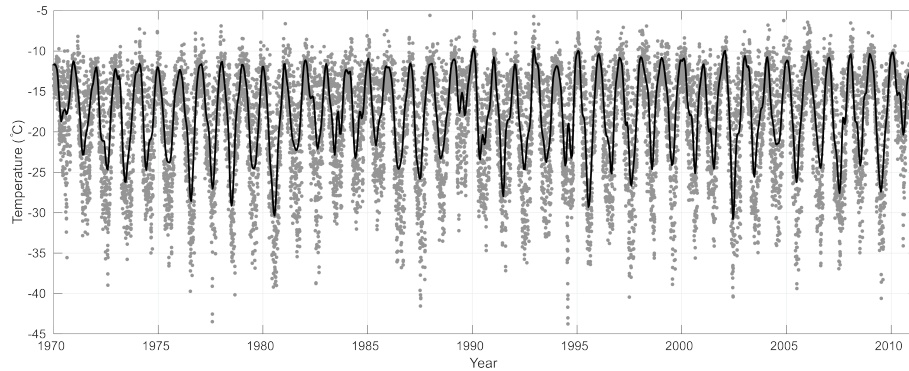
Figure 3. The grey dots are the interpolated and decimated temperature time series $T(t)$. The solid curve is its smoothed and gained counterpart $\mathcal{T}(t)$.

3 Results

3.1 Warping H$_2$O$_2$ concentration data onto the Temperature Series

Figures 2 and 3 conspicuously show that the $\mathcal{C}(z)$ and $\mathcal{T}(t)$ data series record the passing of the years through their annual cycles of peaks and troughs, summer to winter respectively. Nevertheless the two data series do record the annual cycles in distinct manners, the former against depth and the latter against time, their similar shapes suggesting we could employ a simple mapping procedure from depth to year of deposition to a common variable related to time.

Two issues to consider here: (i) $\mathcal{C}(z)$ and $\mathcal{T}(t)$ have their respective zeniths at a given summer on distinct dates, as they are distinct phenomena, and (ii) the shape of the two data series conspicuously differ from each other in terms of their spectral characteristics as easily seen comparing Figures 2 and 3. The first issue is easily dealt with as peaks will differ from each other within a fraction of a given summertime, a noise source one just needs to be aware of. The second point is more involved as $\mathcal{T}(t)$ is a function of time with a nearly constant frequency content throughout, whereas $\mathcal{C}(z)$ has a frequency scaling with depth, a chirp behavior easily seen in Figure 2. The latter results from the gradual thinning of the firn layers due to the weight of the overburden.

The two data series $\mathcal{C}(z)$ and $\mathcal{T}(t)$ are not directly comparable, being functions of depth and time. We can make them comparable though by using a standardizing mapping procedure,

$$
\begin{aligned}
\mathcal{C}_i &\longmapsto \widehat{\mathcal{C}}_i = \tfrac{1}{\sigma(\mathcal{C}_i)}\left(\mathcal{C}_i - \overline{\mathcal{C}}\right) \\
\mathcal{T}_i &\longmapsto \widehat{\mathcal{T}}_i = \tfrac{1}{\sigma(\mathcal{T}_i)}\left(\mathcal{T}_i - \overline{\mathcal{T}}\right),
\end{aligned}
\tag{1}
$$

where $\mathcal{C}_i \equiv \mathcal{C}(z)$ and $\mathcal{T}_i \equiv \mathcal{T}(t)$, $i = 1,\ldots,N$. The $\overline{\mathcal{C}}$ and $\overline{\mathcal{T}}$ are averages and $\sigma(\mathcal{C}_i)$ and $\sigma(\mathcal{T}_i)$ are standard deviations. The two standardized series, $\widehat{\mathcal{C}}$ and $\widehat{\mathcal{T}}$, have the same number of data points and are zero-mean with unit standard deviation. The standardization process minimizes eventual $y-$axis discrepancies between the two series, dwindling the possibility of

misalignment by the DTW algorithm. The mapping (1) is invertible, allowing to go back to the original values whenever needed.

Warp the series $\widehat{\mathcal{C}}$, call it the sample, onto the reference series, $\widehat{\mathcal{T}}$, allowing for layer thinning with depth in the sample. In applying DTW we construct a warp path $W = (w_1, w_2, \ldots, w_K)$ between sample and reference, where each path element w_k is linked to the two series indexes (i, i'), for the N elements in $\widehat{\mathcal{C}}$ and $\widehat{\mathcal{T}}$, respectively. The warp path length W is bounded to $N \leq K \leq 2N - 1$ and subject to the criteria below.

- Boundary conditions: The warp path start and end at the first and the last elements of the two sequences, $w_1 = (1, 1)$ and $w_K = (N, N)$, all elements considered.

- Continuity: The warping procedure preserves the ordering of the two aligned sequences.

$$w_k (i, i') \rightarrow w_{k+1} \left(\widehat{i}, \widehat{i'} \right) \Rightarrow i \leq \widehat{i} \leq (i + 1) \text{ and } i' \leq \widehat{i'} \leq (i' + 1),$$

- Monotonicity: The elements of W are monotonically spaced in the independent variable, thus preventing big jumps.

$$w_k (i, i') \rightarrow w_{k+1} \left(\widehat{i}, \widehat{i'} \right) \Rightarrow \left(i - \widehat{i} \right) \geq 0 \text{ and } \left(i' - \widehat{i'} \right) \geq 0.$$

The process of warping the sample onto the reference series is done through seeking the path W which yields the minimum-distance,

$$D_W = \frac{1}{2N} \min \left\{ \sum_{k=1}^{K} d(w_k, w_{k+1}) \right\}, \tag{2}$$

where $d(w_k, w_{k+1})$ is the distance between two contiguous elements. DW should attain its minimum when the sample is corrected warped onto the reference signal (Sakoe and Chiba, 1978). We do the DTW through with an algorithm using a correlation optimized warping, or COW, which aligns the sample onto the reference by piecewise linear stretching and compression of the warping segments with variable lengths l (Nielsen et al., 1998; Pravdova et al., 2002; Tomasi et al., 2004). The range of possible segments l is limited by an integer slack parameter, initially set to unity, $\mathfrak{s} = 1$. The reconstructed sample is obtained by retaining only the highest values obtained for the cumulative correlation coefficient,

$$\xi \left(\widehat{\mathcal{T}}, \widehat{\mathcal{C}} \right) = \frac{\sum_l \left(\widehat{\mathcal{T}_{i'}} - \overline{\widehat{\mathcal{T}}} \right) \left(\widehat{\mathcal{C}_i} - \overline{\widehat{\mathcal{C}}} \right)}{(M - 1) \sigma \left(\widehat{\mathcal{T}_{i'}} \right) \sigma \left(\widehat{\mathcal{C}_i} \right)}, \tag{3}$$

where the summation is performed for each segment l with M points, $\overline{\widehat{\mathcal{T}}}$ and $\overline{\widehat{\mathcal{C}}}$ are averages, and $\sigma \left(\widehat{\mathcal{T}_{i'}} \right)$ and $\sigma \left(\widehat{\mathcal{C}_i} \right)$ are standard deviations. The problem is solved by applying the COW algorithm on all N/l segments through dynamic programming (Nielsen et al., 1998; Pravdova et al., 2002; Tomasi et al., 2004). A complete description of the DTW and COW algorithms is well beyond the scope of this work, the reader is kindly referred to the literature cited herein.

The analysis proceeds as follows: Begin the process of warping $\widehat{\mathcal{C}}$ onto $\widehat{\mathcal{T}}$ with the two series aligned at their respective beginnings: the borehole bottom and January 1st, 1970, respectively. Warp $\widehat{C}$ and retain the value of the total distance D_W. Discard the year 1970 on $\widehat{\mathcal{T}}$, which now begins on January 1st, 1971 and repeat the warping procedure with the entire $\widehat{C}$ record; retain the new vaule for the total distance D_W. Continue moving forward the beginning of the $\widehat{T}$ record in one year steps, storing the values of D_w estimated at each iteration. Continue this process of advancing the beginning the $\widehat{\mathcal{T}}$ in one year steps, monitoring the evolution of the estimated values of D_w.

We observed a decreasing trend in the estimates of D_w retained at each round of warping described above, which reached a conspicuous minimum with the begining of the $\widehat{\mathcal{T}}$ series aligned on January 1st, 1980. Further one-year steps on the starting date of the temperature ensued an increasing trend with a faster pace. We stopped the one-year step warping process on the ~~incresing~~ increasing branch of D_w five years after reaching its minimum. Figure 4 shows both the original and warped versions of series $\widehat{C}$, with the borehole bottom, aligned with $\widehat{T}$ on January 1st, 1980. The Figure also shows the behavior of D_w for the entire year span we have considered in our calculations.

Once $\widehat{T}$ is warped onto $\widehat{C}$ one can easily perform an inverse mapping to the original depths and time, $i = 1, \ldots, N \mapsto (t; z)$. With that depths may be mapped onto time, directely yielding a borehole time scale, $z = z(t)$. That is is shown in the lower panel of Figure 4 where $\widehat{C}$ is plotted against deposition time in years. The conspicuous minimum on D_w suggests a quantitative error estimate of $\lesssim 1$year, significantly greater than any eventual difference between the time of occurrence of the peaks in $\widehat{C}$ and $\widehat{T}$ within a given year.

3.2   Estimating a Borehole Time Scale and ~~an~~ Accumulation Rate

A simple model of an ice sheet flow considers that as ~~an~~ a year's snowfall moves downward relative to the surface during its burial process by subsequent deposition undergoing viscoplastic deformation, becoming progressively thinner, extending laterally due to ice incompressibility. An increase in density does ensue with depth as snow slowly compacts itself into firn and from that into ice. One way to simplify the process is to express all lengths in water-equivalent units (mweq), thus allowing one to disregard the compaction of snow *before* the complete transformation to ice. Accordingly we present depths as $z_{mweq} = z\,\rho(z)/\rho_w$, where $\rho(z)$ and ρ_w are the density measured in the ice cores from ~~PD~~ DP and of pure water, respectively.

We use the measured $\rho(z)$ from the ice cores to estimate an empirical model of firn densification which assumes the density change with depth is proportional to the deviation relative to the density of pure glacier ice $\rho_{ice} = 0.91 g/cm^3$ (Cuffey and Paterson, 2010). The model may have two (Herron and Langway Jr, 1980) or even three (Ligtenberg et al., 2011) distinct firn densification stages, spanning from the surface to the zone of pore close-off. The adopted model has one densification stage from the surface down to the last available density estimate at $z_{\rho(\max)} = 64.5$m: $\rho_z = 0.339\,z^{0.1853}$, with $R^2 = 0.97$ (Travassos et al., 2018). The density measurements beyond $z_{\rho(\max)}$ were accidentally lost so we impose the density of glacier ice to the borehole bottom, $\rho(109\text{m}) = \rho_{ice}$, bridging the data gap with a straight line linking the imposed value to the last measured density. This extrapolation will result in some inaccuracies but as at $z_{\rho(\max)} = 64.5$m the power law has already reached its slowest increase rate with depth, it may be reasonable to assume they are relatively small. On the other hand that allows
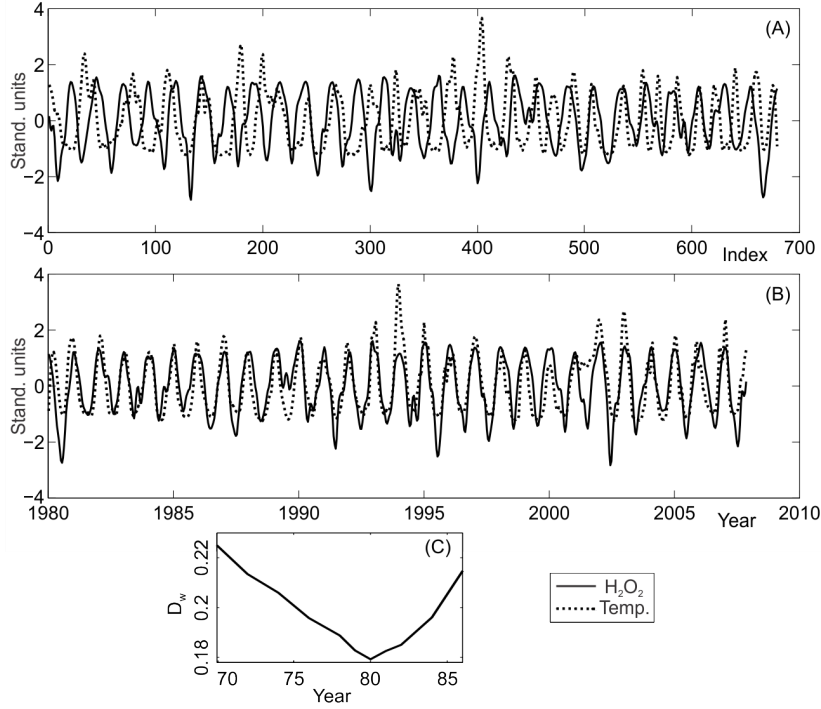
Figure 4. Panel (A) shows the unwrapped $\widehat{C}$ and $\widehat{T}$ series in standardized ordinates, the index $i = 0$ corresponding to the mouth of borehole. Panel (B) shows the two warped series with their abscissas i mapped back to time, expressed in years beginning on January 1st, 1980: $\mathcal{T}, \mathcal{C}(t)$. In both panels $\widehat{C}$ is shown as a dotted curve and $\widehat{T}$ shown as a dash curve, ordinates in arbitrary units. Panel (C) shows the behavior of distance D_w for the year span we have performed the wrappings.

for the transformation of length dimensions to mweq for the entire borehole. We will bring this issue back below whenever appropriate.

In the simplest model for an ice sheet flow the total vertical strain of any layer is equal to the total vertical strain of the ice beneath it,

$$\frac{\lambda(z)}{\lambda_0} = \frac{(1-z)}{h}, \tag{4}$$

of a layer of thickness $\lambda(z)$ since it has been deposited at the surface as an annual layer λ_0 thick and h is the total ice thickness. The model considers a steady state viscoplastic deformation with depth at the center of an ice sheet, as the annual layers are buried by subsequent deposition. From now on all length dimensions are in mweq, unless explicitly said otherwise. As the ice sheet is in a steady state we assume that accumulation and vertical thinning are constant in time and that a layer thickness does not vary horizontally. If those assumptions hold the distance an ice particle moves downwards during one year must be equal to the thickness of one annual layer $\lambda(z)$.

225   As the older ice is closer to the bedrock, it is more convenient to express the vertical position of an ice particle in relation to the rock bed interface using a new vertical axis, $Z = h - z$. The new coordinate frame runs in the opposite direction to the one we have been using so far with $z > 0$ pointing downwards. Assuming a steady state the distance an ice particle moves downwards in one year, or for that matter, the particle vertical velocity $\nu(Z)$, is a linear function on Z and therefore the thinning rate $\mathrm{d}\nu/\mathrm{d}Z$ is constant. The velocity at the surface equals the accumulation rate $\nu(h) = -a$ and at the bed $\nu(0) = 0$,
230 the velocity being negative in the new reference frame as it points downwards,

$$\nu(Z) = -a\frac{Z}{h}. \tag{5}$$

    The relation between a given depth Z to the age of ice is given by

$$t = \int_{h}^{Z} \nu^{-1}\mathrm{d}Z \longrightarrow Z = h\exp\left(-\frac{a}{h}t\right), \tag{6}$$

known as Nye's time scale (Nye, 1952, 1963; Cuffey and Paterson, 2010). Relation (6) provides the simplest model for
235 describing how a layer of thickness λ_0 deposited at the surface thins to $\lambda(Z)$ when it is at a distance Z from the ~~bed~~bedrock. Notwithstanding its simplicity the Nye model still provides good estimates at shallow depths which are close to the ones from more complex models, such as the Dansgaard-Johnsen model (Dansgaard and Johnsen, 1969; Cuffey and Paterson, 2010).

    The warping of $\widehat{C}$ onto $\widehat{T}$ estimates the deposition thickness λ_0 from its observed thickness $\lambda(z)$, therefore reconstructing the accumulation as well as yielding a time scale $z(t)$ spanning the entire borehole. The ~~$z(t)$ is shown in Figure 5 is a spline~~
240 ~~linking the center of each corrected, warped, thickness λ_0 against time. The beginning of the extrapolated densities beyond 64.5m, shows as a subtle inflection at $\sim$ 1990.~~

~~The annual~~ accumulation over the period 1980-2008 as revealed by the warped thicknesses λ_0 show wider oscillations towards later years~~, but their~~. An 11-year moving average ~~, $\bar{a}_{11y} \cong 2.5\,\mathrm{m\,w.e.}/\mathrm{y}$ appears fairly stable~~ on accumulation we indicates a fairly stable regime for the period 1980-2008~~,~~, $\bar{a}_{11y} \cong 2.5\,\mathrm{m\,w.e.}/\mathrm{y}$. The small relative increase in accumulation
245 from 1980-1990 to 1990-2008 seen in Figure 5 ~~also shows the~~ is affected by the estimated densities deeper than 64.5m used to transform depths. Moreover the statistical significance of an 11-year ~~annual accumulation estimated at Gomez in the south-western Antarctic Peninsula (Thomas et al., 2008), showing that a_{ma} is more than twice as large, a very high accumulation rate~~moving average within a 28y time period is limited, we use it for sake of comparison with literature results, where the solar cycle period is often used.

250   Apply an exponential regression on the warped data to produce estimates for the two constants $(h, a/h)$ in relation (6). As the available data is confined to the firn layer an estimate for the total thickness h is obviously beyond our reach. Nevertheless as annual accumulation rate is assumed uniform we can obtain an estimate for the the 27 years prior to the coring activity, $a_N = 2.82\,\mathrm{mweq}/\mathrm{y}$. Peak counting on Figure 2 yields an estimated accumulation of $a_c = 2.5\,\mathrm{m\,w.e.}/\mathrm{y}$, equals to a figure reported elsewhere (Potocki et al., 2016). The two accumulation rate estimates, a_N and $\bar{a}_{11y}$ ~~are compatible, providing a~~ differ by
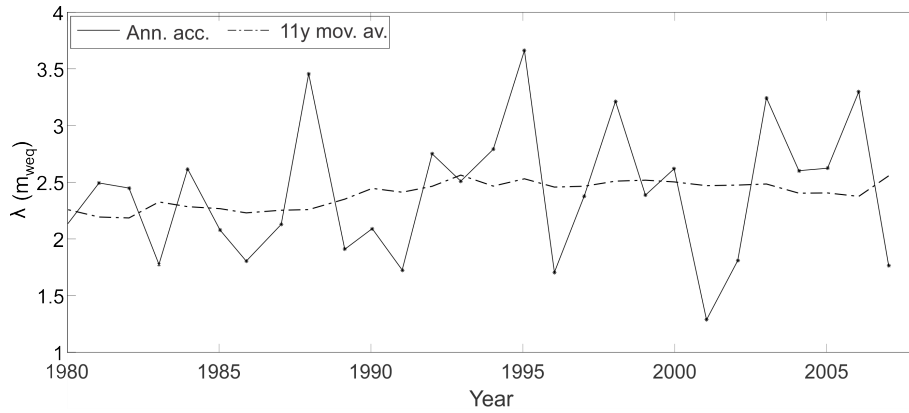
Figure 5. The solid line shows the ~~time scale~~ $z(t)$ ~~(left ordinate) for the firn layer at PD. The dash line shows the~~ annual accumulation rate estimates ~~,~~ at DP and the dot-dash line ~~giving~~ gives their 11-year moving average~~(~~. Use right ordinate ~~). The lower dot line shows the 11-year moving average of~~ for the annual accumulation rate ~~(right~~ and the left ordinate ~~)~~ at ~~Gomez~~ for ~~comparison (Thomas et al., 2008)~~ borehole depths.

255 $\approx 10\%$ being reasonably compatible, considering the assumptions leading to relation (6) and providing a weak check on our numerical procedure.

It is worthwhile to end this section by comparing our estimated annual accumulation variability with data from the three ice cores listed in Table 1, all South of DP in the Antarctic Peninsula. Figure 6 shows that the accumulation rates at DP and Bruce Plateau are compatible throughout, an indication that both sites may have been subject to similar high accumulation
260 regimes, twice as large as Gomez's. The Figure 6 also suggests annual snow accumulation for the period 1980-2010 a stable accumulation for all four ice cores. Nevertheless the time period spanned by our data is too short to probe multi-decadal trends, it is reported that the Antarctic Peninsula has been experiencing an increased rate since 1900 (Thomas et al., 2017). In particular the Bruce Plateau ice core suggests an increase in snow accumulation during the late twentieth century, increasing at a rate of $0.19\,\mathrm{mm}\,\mathrm{w.e.}/\mathrm{y}$ since the 1950s (Goodwin et al., 2016).

Table 1. Location of third party ice cores sites on the Antarctic Peninsula with their distances to DP ice core. z_{max} is the maximum depth and the time span ΔT, in years, is shown between square brackets.

Name	Latitude	Longitude	Elevation(m)	$z_{max}(m)[\Delta T]$	Distance(km)	Reference
Bruce Plateau	-66.0	-64.1	1976	448[1750–2009]	302	(Goodwin et al., 2016)
Dyer Plateau	-70.7	-64.9	2002	190[1504–1990]	767	(Thompson et al., 1994)
Gomez	-73.6	-70.4	1400	136[1858–2006]	1137	(Thomas et al., 2008)
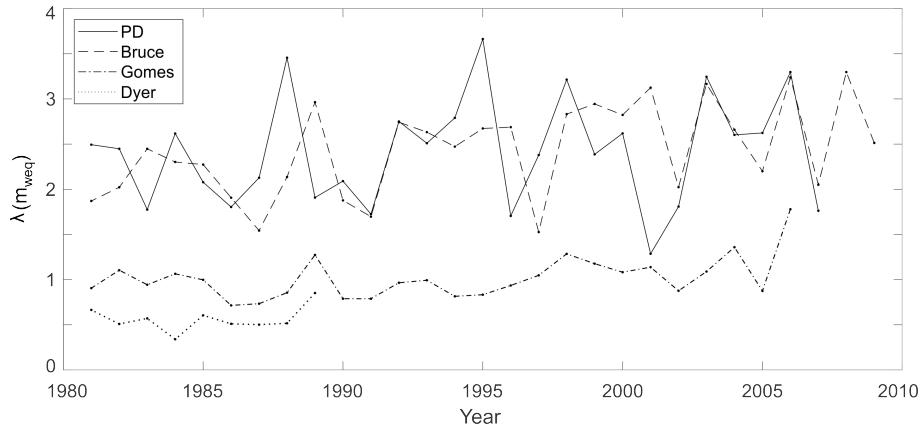
Figure 6. Annual snow accumulation in ice cores from the Antarctic Peninsula region between 1980 and 2010. DP refers to the results of this paper.

265 4   Conclusions

~~We have produced~~ Stratigraphic dating of ice cores is rooted on the use of reference horizons and annually resolved data to count annual layers to establish a core chronology. The latter uses outward data, *e.g.* volcanic events, to count annual layers. This work has resorted to an independent dataset, recorded temperature series as time reference to reconstruct a given layer thickness λ_0 at the deposition time from its observed thickness $\lambda(z)$, thus reconstructing the annual accumulation, thereby a
270 time scale, an ice-core chronology $z(t)$ ~~, for the 133m deep borehole~~.

We have demonstrated that with H_2O_2 concentration data series measured on 98m worth of ice cores from borehole DP-07-1 ~~drilled in Plateau Detroit, Antarctic Peninsula. $z(t)$ is a direct outcome from the process of warping a high resolution H_2O_2 concentration data series~~ dug by us on the central ice divide of DP. We adopted a non-linear numerical algorithm which warped the concentration data onto an estimated local temperature ~~time series. The~~ record by aligning their respective summertime
275 peaks, an interannual process with a $\simeq 0.5y$ time accuracy. The viability and the physical reliability of the procedure ~~is rooted~~ are rooted both on the robustness of H_2O_2 as a seasonal marker ~~in a location of high accumulation , which in turn brought the borehole depth span~~ associated to the observed high accumulation rate, which brought the entire borehole to within the operational life span of the Antarctic stations. ~~The non-linear warping of the concentration data onto the estimated temperature record allowed for correcting the thinning of annual layers due to the vertical strain with depth of the firn layers, to obtain an~~
280 ~~estimate of their thicknesses at the time of snow deposition.~~

The considerable noise content on both series were alleviated through a loess nonparametric filter, which produced clean smoothed versions of the data series albeit still retaining their complexity, as seen in Figures 2 and 3. Any time difference between the summertime temperature and peroxide concentration peaks fall necessarily within the interannual process' time accuracy of $\simeq 0.5y$. The whole process was based on numerical optimization, producing a mathematically sound match
285 between the two series.

~~With the warping procedure the annual layers, as revealed through a series of peaks and troughs on the H_2O_2 series, have their thicknesses corrected to their original values at the year of snow deposition. The reconstructed thickness built during one year is equals to~~ The secular variation in accumulation has revealed a high annual accumulation rate of $a_N = 2.8\,\mathrm{mweq/y}$, with the large variability seen in Figure 5. The observed high accumulation rate at DP is of the same order of the one reported for Bruce Plateau, being highly correlated with each other throughout the observational period considered here. The DP regime shows one year earlier than at Bruce in a couple of time sections in Figure 6, a small but detectable discrepancy, probably related to the ~~annual accumulation rate. An 11-year moving average of the reconstructed annual layer thicknesses displays distinct dating approaches.~~ The conspicuous correlation of DP and Bruce is as indication that the Northern tip of the Antarctic Peninsula has been under a high snow accumulation regime, twice as large as Gomez's further South. The short time span reported here is incapable of revealing multi-decadal trends nevertheless it is reasonable to suggest the DP may have been experiencing a similar increase in snow accumulation in the late twentieth century, similar to the one reported at Bruce Plateau.

The limited time window of the time span of our data reveals a fairly stable behavior throughout the 27 years prior to coring, with an 11-year moving average on accumulation of $\bar{a}_{11y} \cong 2.5\,\mathrm{m\ w.e./y}$~~. Regressing the same data using the exponential expression of Nye's time scale yields another estimate for the annual accumulation rate, $a_N = 2.82\,\mathrm{m\,w.e./y}$. Those two estimates may be regarded as defining a range for a very high annual accumulation rate. That range points to an accumulation rate more than 3 times the one reported at Gomez in the south-western Antarctic Peninsula $0.8\,\mathrm{mweq/y}$ (Thomas et al., 2008)~~, a regularity in snow deposition which preserved a reliable climate record, minimizing post-depositional losses on the concentration of H_2O_2. By the same token we should expect a tight temporal range of ice cores in the northern Antarctic Peninsula. All that points to that region an important climate laboratory as for coring activity; assuming a deposition rate stability the top DP layer should be now, almost 15 years after, half way through the firn layer.

~~By the same token we have taken advantage of the strong seasonality on H_2O_2 data and the high accumulation rate to perform the warping procedure we could have used them to estimate~~ Mathematical procedures for annual layer counting are notoriously laborious as compared to manual counting, nevertheless the latter has no other intrinsic quality but its easiness; quality or effectiveness cannot be technically guaranteed. The former approach, as is the case of the present work, is indisputably rigorous, able to estimate efficiently the annual layering on the entire data section and is disposition-free. The layer counting on our data produced annual accumulation figures that differ from the ones presented here up to 40%, being 17% on average. All that considered the choice ultimately remains with the investigator weighing in on an acceptable level of chronological inaccuracy to his work.

Comparison of algorithm results with simple layer counting performed on the smoothed versions of our dataset suggests inaccuracies are non-uniform and within $\sim \pm 1y$. Notwithstanding the algorithm is potentially useful on other datasets where manual counting is more challenging than in the present case, it is not case-specific and it is not restricted to the ~~mean annual accumulation rate by straightforwardly counting the peroxide annual cycles. If one counted the peaks in Figure 2 one would have estimated an accumulation of $a_c = 2.5\,\mathrm{m\ w.e./y}$ as it is reported elsewhere (Potocki et al., 2016). On the other hand one would not have been able to retrieve the time-corrected layer thickness accumulated at the surface at a given year λ_0. All~~

~~the results related to the accumulation at PD were obtained through a mathematical optimization process, without human intervention~~dyad peroxide-temperature either; it can deal with other kinds of annually laminated data, not necessarily of related origin, even among distinct wells. We are convinced there may be many other situations where there is the need of synchronization of distinct datasets where the procedure shown here may prove useful.

325 *Author contributions.* J. Travassos worked with the synchronization of H_2O_2 and temperature data series and its accrued accumulation rate, and wrote the manuscript. S. Martins estimated the temperature data series and contributed with additional data processing. M. Potocki processed the original H_2O_2 data series from the ice cores. J. Simões worked with all aspects of acquiring the ice cores in the field and contributed with several glaciological aspects of this work. All authors reviewed and agreed on the final manuscript.

Acknowledgements. This work was fully supported by the Brazilian Antarctic Program (PROANTAR), through the CNPq and CAPES. The
330 two main sources come from the INCT da Criosfera (CAPES Proj. 88887.136384/2017-00) and PROANTAR/CNPq (Proj. 442755/2018-0). The present work is part of the ice core program Climate of Antarctica and South America (CASA) in association with the Climate Change Institute, University of Maine. Authors also acknowledge the logistical support of the Chilean Antarctic Institute/INACH and the Chilean Air Force/FACh, the Brazilian Air Force and Navy.

References

335   Capron, E., Landais, A., Lemieux-Dudon, B., Schilt, A., Masson-Delmotte, V., Buiron, D., Chappellaz, J., Dahl-Jensen, D., Johnsen, S., Leuenberger, M., et al.: Synchronising EDML and NorthGRIP ice cores using δ 18 O of atmospheric oxygen (δ 18 O atm) and CH 4 measurements over MIS5 (80–123 kyr), Quaternary Science Reviews, 29, 222–234, 2010.

Chaovalitwongse, W. and Pardalos, P.: On the time series support vector machine using dynamic time warping kernel for brain activity classification, Cybernetics and Systems Analysis, 44, 125–138, 2008.

340   Cleveland, W. S. and Grosse, E.: Computational methods for local regression, Statistics and Computing, 1, 47–62, 1991.

Criel, J. and Tsiporkova, E.: Gene Time Eχpression Warper: a tool for alignment, template matching and visualization of gene expression time series, Bioinformatics, 22, 251–252, 2005.

Cuffey, K. and Paterson, W.: Physics of Glaciers, 4th Edn, 2010.

Dansgaard, W. and Johnsen, S.: A flow model and a time scale for the ice core from Camp Century, Greenland, Journal of Glaciology, 8,

345   215–223, 1969.

Frey, M. M., Bales, R. C., and McConnell, J. R.: Climate sensitivity of the century-scale hydrogen peroxide (H2O2) record preserved in 23 ice cores from West Antarctica, Journal of Geophysical Research: Atmospheres, 111, 2006.

Gilbert, J. M., Rybchenko, S. I., Hofe, R., Ell, S. R., Fagan, M. J., Moore, R. K., and Green, P.: Isolated word recognition of silent speech using magnetic implants and sensors, Medical engineering & physics, 32, 1189–1197, 2010.

350   Gillet-Chaulet, F., Gagliardini, O., Seddik, H., Nodet, M., Durand, G., Ritz, C., Zwinger, T., Greve, R., and Vaughan, D. G.: Greenland ice sheet contribution to sea-level rise from a new-generation ice-sheet model, The Cryosphere, 6, 1561–1576, 2012.

Goodwin, B. P., Mosley-Thompson, E., Wilson, A. B., Porter, S. E., and Sierra-Hernandez, M. R.: Accumulation variability in the Antarctic Peninsula: The role of large-scale atmospheric oscillations and their interactions, Journal of Climate, 29, 2579–2596, 2016.

Herron, M. M. and Langway Jr, C. C.: Firn densification: an empirical model, Journal of Glaciology, 25, 373–385, 1980.

355   Hutterli, M. A., McConnell, J. R., Bales, R. C., and Stewart, R. W.: Sensitivity of hydrogen peroxide (H2O2) and formaldehyde (HCHO) preservation in snow to changing environmental conditions: Implications for ice core records, Journal of Geophysical Research: Atmospheres, 108, 2003.

Kolhe, S. R., Patil, P. M., et al.: Dynamic time warping based static hand printed signature verification, Journal of Pattern Recognition Research, 1, 52–65, 2009.

360   Latecki, L. J., Megalooikonomou, V., Wang, Q., and Yu, D.: An elastic partial shape matching technique, Pattern Recognition, 40, 3069–3080, 2007.

Legrand, B., Chang, C., Ong, S., Neo, S.-Y., and Palanisamy, N.: Chromosome classification using dynamic time warping, Pattern Recognition Letters, 29, 215–222, 2008.

Ligtenberg, S., Heilsen, M., and van de Broeke, M.: An improved semi-empirical model for the densification of Antarctic firn, The

365   Cryosphere, 5, 809–819, 2011.

Masson-Delmotte, V., Dreyfus, G., Braconnot, P., Johnsen, S., Jouzel, J., Kageyama, M., Landais, A., Loutre, M.-F., Nouet, J., Parrenin, F., et al.: Past temperature reconstructions from deep ice cores: relevance for future climate change, 2006.

Nielsen, N.-P. V., Carstensen, J. M., and Smedsgaard, J.: Aligning of single and multiple wavelength chromatographic profiles for chemometric data analysis using correlation optimised warping, Journal of Chromatography A, 805, 17–35, 1998.

370   Nye, J.: The mechanics of glacier flow, Journal of Glaciology, 2, 82–93, 1952.

Nye, J.: Correction factor for accumulation measured by the thickness of the annual layers in an ice sheet, Journal of Glaciology, 4, 785–788, 1963.

Passalacqua, O., Gagliardini, O., Parrenin, F., Todd, J., Gillet-Chaulet, F., and Ritz, C.: Performance and applicability of a 2.5-D ice-flow model in the vicinity of a dome, 2016.

375 Potocki, M., Mayewski, P. A., Kurbatov, A. V., Simoes, J. C., Dixon, D. A., Goodwin, I., Carleton, A. M., Handley, M. J., Jaña, R., and Korotkikh, E. V.: Recent increase in Antarctic Peninsula ice core uranium concentrations, Atmospheric Environment, 2016.

Pravdova, V., Walczak, B., and Massart, D.: A comparison of two algorithms for warping of analytical signals, Analytica Chimica Acta, 456, 77–92, 2002.

Rabiner, L., Rosenberg, A., and Levinson, S.: Considerations in dynamic time warping algorithms for discrete word recognition, IEEE
380 Transactions on Acoustics, Speech, and Signal Processing, 26, 575–582, 1978.

Rolland, C.: Spatial and seasonal variations of air temperature lapse rates in Alpine regions, Journal of Climate, 16, 1032–1046, 2003.

Sakoe, H. and Chiba, S.: Dynamic programming algorithm optimization for spoken word recognition, IEEE transactions on acoustics, speech, and signal processing, 26, 43–49, 1978.

Sigg, A. and Neftel, A.: Seasonal variations in hydrogen peroxide in polar ice cores, Ann. Glaciol, 10, 157–162, 1988.

385 Steig, E. J., Mayewski, P. A., Dixon, D. A., Kaspari, S. D., Frey, M. M., Schneider, D. P., Arcone, S. A., Hamilton, G. S., Spikes, V., Albert, M., et al.: High-resolution ice cores from US ITASE (West Antarctica): Development and validation of chronologies and determination of precision and accuracy, Annals of Glaciology, 41, 77–84, 2005.

Thomas, E. R., Marshall, G. J., and McConnell, J. R.: A doubling in snow accumulation in the western Antarctic Peninsula since 1850, Geophysical research letters, 35, 2008.

390 Thomas, E. R., Van Wessem, J. M., Roberts, J., Isaksson, E., Schlosser, E., Fudge, T. J., Vallelonga, P., Medley, B., Lenaerts, J., Bertler, N., et al.: Regional Antarctic snow accumulation over the past 1000 years, Climate of the Past, 13, 1491–1513, 2017.

Thompson, L., Peel, D., Mosley-Thompson, E., Mulvaney, R., Dal, J., Lin, P., Davis, M., and Raymond, C.: Climate since AD 1510 on Dyer Plateau, Antarctic Peninsula: Evidence for recent climate change, Annals of Glaciology, 20, 420–426, 1994.

Tomasi, G., Van Den Berg, F., and Andersson, C.: Correlation optimized warping and dynamic time warping as preprocessing methods for
395 chromatographic data, Journal of Chemometrics, 18, 231–241, 2004.

Travassos, J. M., Martins, S. S., Simões, J. C., and Mansur, W. J.: Radar diffraction horizons in snow and firn due to a surficial vertical transfer of mass, Brazilian Journal of Geophysics, 36, 507–518, 2018.

Verbesselt, J., Hyndman, R., Newnham, G., and Culvenor, D.: Detecting trend and seasonal changes in satellite image time series, Remote sensing of Environment, 114, 106–115, 2010.

400 Vinther, B. M., Clausen, H. B., Johnsen, S. J., Rasmussen, S. O., Andersen, K. K., Buchardt, S. L., Dahl-Jensen, D., Seierstad, I. K., Siggaard-Andersen, M.-L., Steffensen, J. P., et al.: A synchronized dating of three Greenland ice cores throughout the Holocene, Journal of Geophysical Research: Atmospheres, 111, 2006.

Wang, K., Gasser, T., et al.: Alignment of curves by dynamic time warping, The annals of Statistics, 25, 1251–1276, 1997.

Winstrup, M. and Svensson, A.: An Automated Method for Annual Layer Counting in Ice Cores, 2010.

405 Xue, Z., Du, P., and Feng, L.: Phenology-driven land cover classification and trend analysis based on long-term remote sensing image series, IEEE Journal of Selected Topics in Applied Earth Observations and Remote Sensing, 7, 1142–1156, 2014.